Full-Duplex in a Hand-Held Device – From Fundamental Physics to Complex Integrated Circuits, Systems and Networks: An Overview of the Columbia FlexICoN Project

Harish Krishnaswamy, Gil Zussman, Jin Zhou, Jelena Marašević, Tolga Dinc, Negar Reiskarimian, Tingjun Chen
Electrical Engineering, Columbia University, New York, NY 10027, USA
{harish@ee., gil@ee., jz2495, jelena@ee., td2376, nr2475, tingjun@ee.}columbia.edu

***Abstract*—Full-duplex wireless is an exciting emerging wireless communication paradigm that also poses tremendous challenges at virtually every layer: from the antenna interface and integrated circuits (ICs) and systems to the network layer. This paper covers recent advances at Columbia University across all these dimensions. Several potential full-duplex system architectures that are appropriate for different application spaces are discussed. Specific research advances include (i) a novel integrated CMOS non-reciprocal circulator that utilizes time-variance to break Lorentz reciprocity, (ii) a polarization-based antenna cancellation technique that achieves very wideband isolation that can be reconfigured as the environment changes, (iii) several generations of RF and analog self-interference cancellation circuits that combat noise, distortion and bandwidth limitations, (iv) higher-layer resource allocation algorithms that evaluate full-duplex rate gains given realistic physical layer models, and (v) demonstrations of full-duplex operation using realistic IC-based nodes.**

I. Introduction

Full-duplex (FD) communication – simultaneous transmission and reception on the same frequency channel – has been recognized as one of the key technologies on the roadmap to 5G wireless standards [1]. Existing wireless systems are half-duplex, where a single user can either transmit or receive (but not both) in a given frequency and time slot. Thus, FD wireless technology has the potential to substantially improve the utilization of limited wireless spectrum resources.

While an attractive approach that sounds simple as a concept, when it comes to the implementation, FD poses tremendous challenges over both the physical and the medium access control (MAC) layers (for an overview, see [2] and references therein). One of the most fundamental challenges stems from the leakage of the transmitter's signal into the receiver chain – the effect known as self-interference (SI). In many wireless systems, such as Wi-Fi and LTE, the SI signal is billions of times stronger than the useful signal at the receiver, requiring extremely accurate SI cancellation (SIC).

Despite the challenges in achieving extremely high levels of SIC, the feasibility of FD communication was recently established in [3]–[5] by using laboratory bench-top equipment and off-the-shelf components. The goal in [3]–[5] was to bring the FD capability to base stations and infrastructure, where the cost and form factor constraints are not as stringent as in mobile devices. However, meeting the strict requirements for low-cost, small form factor, and/or integrated implementations, which are imperative for transceivers in mobile devices, is challenging More recently, our work [6]–[10] and the works in [11], [12] demonstrated SIC and FD operation within CMOS ICs. To utilize the benefits of these small form factor implementations, a careful redesign of both the physical and MAC layers is necessary.

Therefore, within the "Full-duplex wireless: from Integrated Circuits to Networks" (FlexICoN) project [13], we are taking a holistic cross-disciplinary approach to address the challenges arising across the physical and MAC layers, focusing on the interactions between these two layers. In this paper, we describe some of the recent results obtained within the FlexICoN project and discuss its cross-layer aspects.

II. Integrated FD Transceivers

SI isolation and cancellation in the antenna and analog/RF domains prior to digital SIC are crucial for practical FD implementations with realistic receiver and analog-to-digital converter (ADC) dynamic range requirements. There are several fundamental challenges associated with an integrated FD radio implementation in CMOS, and we describe them in more detail in the following.

A. Antenna Interfaces for Full-Duplex

Existing antenna domain SI suppression works can be divided into two main categories. The techniques in the first category [14], [15] target increasing the T/R isolation by minimizing the inherent TX-to-RX coupling. These approaches lack the ability to combat the variable SI scattering from the environment during in-field operation. The techniques in the second category are essentially based on performing SIC in the antenna domain [16], [17]. However, neither of these techniques demonstrated SIC in a changing electromagnetic environment.

In [9], we proposed a wideband reconfigurable polarization-based antenna cancellation technique (Fig. 1). First, co-located rectangular slot loop TX and RX antennas with orthogonal polarizations are employed to increase initial isolation. Addition-

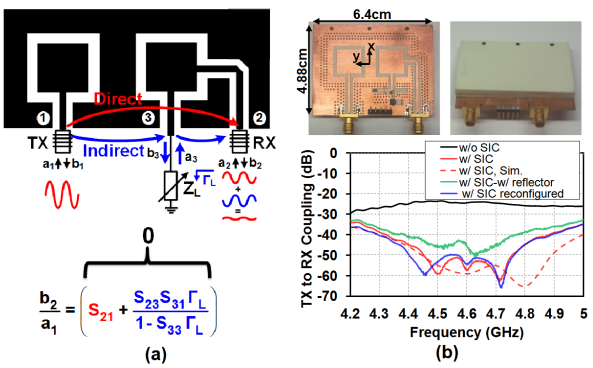

Fig. 1: T/R antenna pair with polarization-based antenna cancellation: (a) concept, (b) 5 GHz prototype and measurements.

ally, an auxiliary port which is co-polarized with the TX antenna is created on the RX antenna and terminated with a high-order reflective termination to perform wideband SIC. The reflective termination is electronically reconfigurable to combat variable environmental reflections. A 4.6 GHz prototype employing this technique achieves more than 50 dB isolation over 300 MHz SIC bandwidth (20x higher than conventional RF cancellers). This high level of isolation is maintained even in the presence of strong nearby reflectors. This technique is readily scalable in frequency and formed the backbone of our 60 GHz full-duplex fully-integrated transceiver in [10]. Such a T/R antenna pair is useful for point-to-point links (microwave or millimeter-wave backhaul) where form factor requirements are somewhat relaxed.

In cases where form-factor is an extreme concern, shared antenna interfaces such as electrical-balance duplexers [18] and circulators are preferable. Reciprocal shared-antenna interfaces such as electrical-balance duplexers suffer from a theoretical 3 dB (practically more) loss; hence more than half of the signal power is lost right at the antenna interface.

Nonreciprocal circulators can potentially offer a low-loss, small form factor antenna interface with high transmitter-receiver (TX-RX) isolation. However, commercial circulators are built using ferrite materials and are bulky, expensive, and cannot be integrated on a CMOS platform.

In [8], [19] we conceived, designed, and fabricated the first CMOS non-magnetic non-reciprocal passive circulator, which uses time-variance to break Lorentz reciprocity and mimic the effect of ferrite materials. *This first CMOS passive non-magnetic circulator simultaneously achieves low loss in both directions, high isolation between TX and RX, small form factor, and high linearity for TX signals*. The concept, implementation, and measurement results of the proposed non-magnetic passive circulator are shown in Fig. 2.

B. Compact Wideband RF Self-Interference Cancellers

One of the fundamental challenges associated with SIC at RF is the cancellation bandwidth due to the frequency selectivity of the antenna interface. A conventional RFIC canceller that we implemented in [6] has a programmable but frequency-flat magnitude and phase response. Thus, the canceller from [6] can only emulate the antenna interface isolation at a single

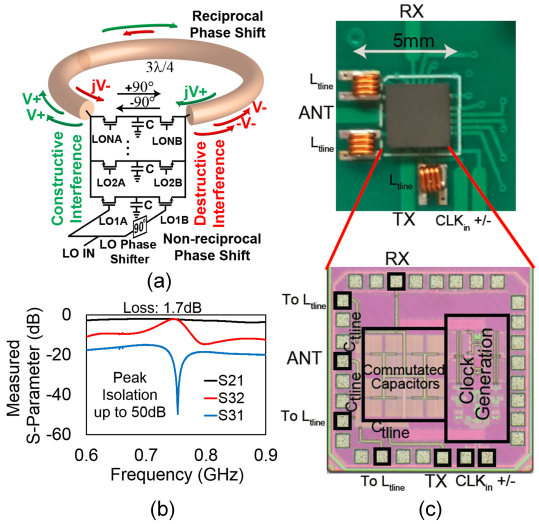

Fig. 2: Passive magnetic-free circulator: (a) concept, (b) S-parameters measurement results, and (c) 65 nm CMOS implementation.

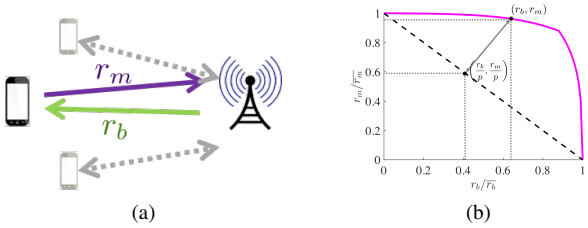

Fig. 3: (a) An FD link and (b) the definition of rate improvement.

frequency point, resulting in a narrowband SIC. Wideband SIC at RF based on time-domain equalization was reported using multiple on-PCB transmission-line delays and variable attenuators [3]. However, generation of nanosecond-scale true time delay on silicon is extremely challenging due to the required transmission line length and the lossy nature of the silicon substrate.

In [7], *we demonstrated integrated SIC in the RF domain using a concept called frequency-domain equalization (FDE)*. The FDE technique employs multiple RF bandpass filters (BPFs) with independent control of their magnitude, phase, center-frequency, and quality factor to emulate the SI channel in different frequency sub-bands. The realization of FDE in the RF domain is accomplished by leveraging modern ultra-scaled CMOS technology – with transistors that are able to be efficiently switched at high frequencies, high-quality factor RF BPFs can be realized based on linear periodically time varying (LPTV) circuits [20]. The concept, implementation, and measurement results of the reported FDE-based FD radio receiver are reported in [7].

III. Algorithms and Rate Gains

For a given profile of residual SI based on the FD transceiver implementations and other wireless system parameters, such as, maximum irradiated power and typical signal-to-noise ratio (SNR) values, it is important to understand how much rate improvement can be attained from the use of FD. On one hand, such results can serve for evaluating different trade-offs

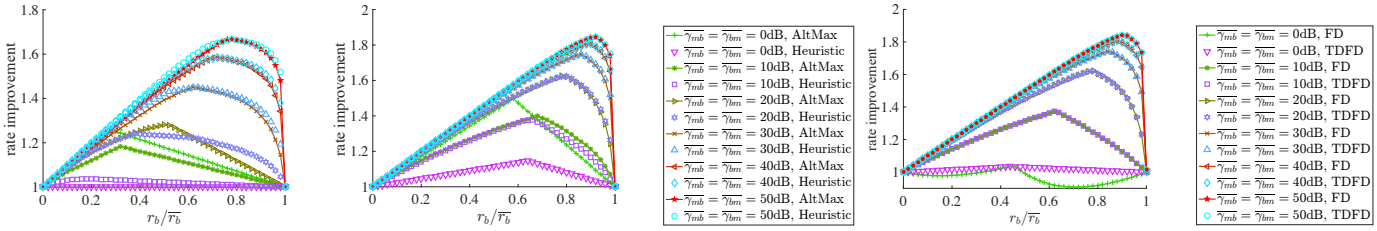

(a) (b) (c)

Fig. 4: (a) Achievable rate improvements for fixed r_b and maximized r_m, for the MS FD receiver from [6], (b) achievable rate improvements for fixed r_b and maximized r_m, for the MS FD receiver from [7], and (c) achievable rate improvements for fixed r_b and maximized r_m, for the MS FD receiver from [7] and equal power allocation. The FD receiver at the BS is assumed to have a frequency-flat residual SI profile, at the level of noise, as in [3].

incurred by incorporating FD in an existing wireless system. For example, a system designer would consider the trade-off between achievable rate improvements and incurred cost and complexity of implementing FD. On the other hand, the ability to quantify achievable rate improvements given wireless system parameters and residual SI can serve as a guideline for developing FD physical layer. For example, given a target FD rate improvement, it is possible to budget the amounts of SIC across different stages of an FD receiver, based on the typical values of SNR and maximum output power in a system.

To provide results that quantify achievable rate improvements from FD under realistic models of residual SI, we performed a thorough analytical, algorithmic, and numerical study in [21]–[23]. In particular, we considered rate improvements for an FD link, as illustrated in Fig. 3(a), where one station is designated as the mobile station (MS), and the other is designated as the base station (BS). We focused on systems with orthogonal channels, such as, e.g., orthogonal frequency division multiplexing (OFDM) systems. We obtained analytical results and developed power allocation algorithms that maximize the sum of the uplink (UL) and downlink (DL) rates over the channels in [21], [22] and also that determine the capacity regions of FD links in [23]. Our results were accompanied by the numerical evaluations for full-duplex rate improvements under measurement-based values of residual SI and realistic wireless system parameters.

To evaluate rate improvements from FD, we used time-division duplex (TDD) systems as a baseline. In TDD systems, different combinations of UL and DL rates are attained through time sharing between HD transmissions on the UL and the DL (the dashed line in Fig. 3(b)). For an UL-DL FD rate pair (r_m, r_b) we defined the FD rate improvement as the number p, such that $(r_m/p, r_b/p)$ is on the boundary of the corresponding TDD capacity region (i.e., $(r_m/p, r_b/p)$ can be obtained through time-sharing between the maximum TDD UL and DL rates; see Fig. 3(b) for an illustration).

Here, we illustrate the results for the FD capacity regions. The capacity region is defined as the set of all achievable (UL, DL) rate pairs, and the problem of determining the capacity region can equivalently be cast as the problem of maximizing one of the (UL and DL) rates when the other rate is fixed. If different (UL, DL) rate pairs are obtained only through different power allocations, the FD capacity region is not convex in general. However, if we allow time sharing between different FD rate pairs, we obtain the convex hull of the FD region, which, in general, leads to higher rates. We refer to such "convexified" region as time-division FD (TDFD) region. We also note that a convex FD capacity region is desirable, as most scheduling algorithms rely on such assumptions.

The problem of determining either FD or TDFD capacity region is non-convex when a general power allocation over OFDM channels is considered. However, we developed an algorithm (AltMax) that determines the TDFD region under mild restrictions and is guaranteed to converge to a stationary point, which in practice is a global optimum. Building upon insights from the power allocation returned by the algorithm for various points on the capacity region, we also developed a simple heuristic with similar performance, but lower running time. The rate improvements obtained by AltMax and the heuristic are illustrated in Figs. 4(a) and 4(b), for the residual SI of the FD receivers implemented in [6], [7] and different values of average UL and DL SNRs. In Fig. 4, we illustrate the rate improvements for equal average SNRs on the UL and DL, denoted by $\overline{\gamma_{bm}} = \overline{\gamma_{mb}}$, assuming frequency-flat fading.[1] Here, "average SNR" refers to the average SNR over frequency channels, when the maximum total irradiated power is split equally among the channels.

As Figs. 4(a) and 4(b) suggest, more broadband cancellation (i.e., using a more broadband canceller from [7] instead of the canceller from [6]) leads to significantly higher rate improvements. Moreover, whenever the rate improvements are high, the problem of determining the capacity regions can be addressed by a simple heuristic. For comparison, we also illustrate the achievable rate improvements for equal power allocation – namely, when power levels are allocated equally among the channels – in Fig. 4(c). As Fig. 4(c) suggests, for sufficiently high SNRs (and, consequently, high rate improvements), equal power allocation provides similar rate improvements to AltMax and the heuristic from [23], and therefore, simple power allocation policies suffice.

[1] Our results are valid for any fading profile and any values of UL-DL SNRs. We focus on simple cases to isolate the effect of FD from other wireless link parameters.

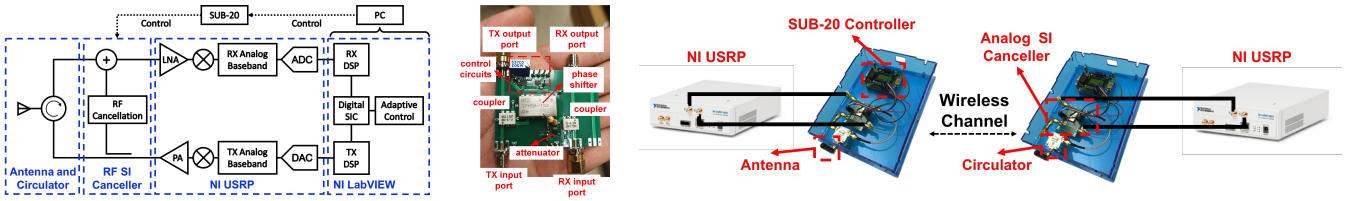

(a) (b) (c)

Fig. 5: (a) Block diagram of the FD transceiver prototype, (b) the 0.8 GHz to 1.3 GHz frequency-flat amplitude and phase-based (conventional) RF SI canceller, and (c) an FD wireless link that is presented in [24], in which each FD transceiver is composed of an antenna, a circulator, a custom-designed RF SI canceller, and an NI USRP.

IV. Full Duplex Testbed and Performance Evaluation

To experimentally evaluate a frequency-flat RF SI canceller of the type reported in [6], we prototyped FD transceivers using the National Instruments (NI) Universal Software Radio Peripherals (USRPs) and our custom-designed discrete-component-based RF SI canceller that emulates its integrated counterpart in [6]. In this section, we describe our full-duplex testbed setup, together with the implemented adaptive RF SIC algorithm and digital SIC algorithm.

A. Setup

The implemented FD transceiver consists of an antenna, a ferrite circulator, a custom-designed RF SI canceller, and an NI USRP. The operating frequency of the NI USRP is configured to be 0.9 GHz, which is the same as the operating frequency of both the circulator and the compact RF SI canceller. The USRP is controlled from a PC that runs NI LabVIEW, which performs digital signal processing.

The diagram of the FD transceiver is shown in Fig. 5(a), in which the RF SI canceller taps a reference signal at the output of the power amplifier (PA) and performs SIC at the input of the low-noise amplifier (LNA) at the RX side. Fig. 5(b) shows the implemented RF SI canceller, in which (i) the attenuator provides an attenuation range from 0 dB to 15.5 dB with a 0.5 dB resolution, and (ii) the phase shifter covers the full 360° range and is controlled by an 8-bit Digital-to-Analog Converter (DAC) with a resolution of about 1.5°. Fig. 5(c) shows the FD wireless link consisting of two FD transceivers that we presented in [24]. In the rest of the section, we describe our adaptive RF SIC algorithm, adaptive digital SIC algorithm, and the FD wireless link demonstration.

B. Adaptive RF SIC Algorithms

The transfer function (TF) of the RF SI canceller depicted in Fig. 5(b) can be modeled as $H = A \cdot \exp(-j\phi)$, in which A and ϕ are the frequency-flat configuration parameters of amplitude and phase that need to be tuned to match that of the antenna interface at the center frequency.

To compute the optimal configuration parameters (A^*, ϕ^*), only two measurements with different (A, ϕ) settings are needed. However, in practice,the unknown RF front-end gain of the USRP complicates the estimation of the amplitude and phase that the RF SI canceller should mimic. Therefore, we implemented the adaptive RF SIC mechanism using four measurement points for the three unknowns (A, ϕ, and the USRP gain) to compute an initial configuration, followed by a local tuning to search for the optimal (A, ϕ). This process consists of two phases.

Initial Configuration: To find the near-optimal initial configuration (A_0, ϕ_0), four measurements are taken with different (A, ϕ) settings: $(0, 0°)$, $(A', 0°)$, $(A', 90°)$, and $(A', 270°)$, where A' is a known attenuation set manually. Let K denote the unknown USRP RF front-end gain and r_i $(i = 1, 2, 3, 4)$ denote the residual signal strength of the i-th configuration, (A_0, ϕ_0) can be found by solving the following equations

$$\begin{aligned} K \cdot (r_1)^2 &= (A_0)^2, \\ K \cdot (r_2)^2 &= (A_0 \cos\phi_0 - A')^2 + (A_0 \sin\phi_0)^2, \\ K \cdot (r_3)^2 &= (A_0 \cos\phi_0)^2 + (A' - A_0 \sin\phi_0)^2, \\ K \cdot (r_4)^2 &= (A_0 \cos\phi_0)^2 + (A' + A_0 \sin\phi_0)^2. \end{aligned}$$

Local Adjustment: From our experiments, the initial configuration provides around 15 dB RF SIC. Therefore, further local tuning around the initial configuration (A_0, ϕ_0) is performed to search for the best performance.

While operating, if the FD transceiver encounters noticeable environmental changes by observing the residual signal strength, it will repeat the process described above to recompute the optimal canceller settings.

C. Digital SIC

The residual SI after isolation and cancellation in the antenna and RF domains is further suppressed in the digital domain. The digital SI canceller is modeled as a truncated Volterra series and is implemented based on a non-linear tapped delay line to cancel both the main SI and the intermodulation distortion generated on the SI. Specifically, the output of the discrete-time SI canceller, y_n, can be written as a function of the current and past TX digital baseband signals, x_n and x_{n-k} (k represents the delay index), i.e.,

$$y_n = \sum_{k=0}^{N} h_{1,k} x_{n-k} + \sum_{k=0}^{N} h_{2,k} {x_{n-k}}^2 + \sum_{k=0}^{N} h_{3,k} {x_{n-k}}^3, \quad (1)$$

in which N corresponds to the maximum delay in the SI channel and $h_{i,k}$ $(i = 1, 2, 3)$ is the i-th order digital canceller coefficient. Depending upon the SI channel, higher order nonlinear terms can be included (the model in (1) only includes

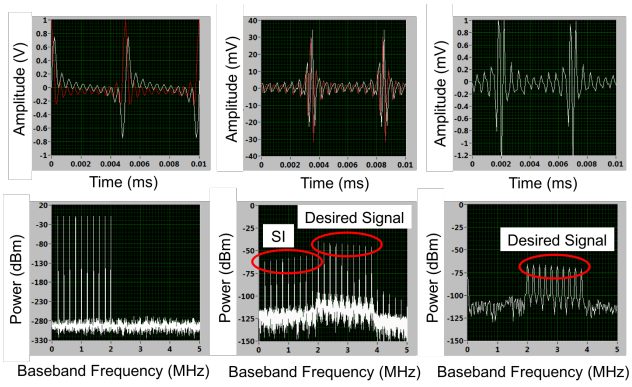

Fig. 6: NI LabVIEW user interface showing the transmitted signal (left column), received signal with desired signal after antenna isolation and RF SIC (middle column), and recovered desired signal after digital SIC (right column).

up to the 3^{rd}-order non-linearity). Using a pilot data sequence, the digital SI canceller coefficients can be found by solving the least-square problem.

D. An FD Wireless Link Demonstration

In [24], we demonstrated that for a $5\,\text{MHz}$ multi-tone signal with $10\,\text{dBm}$ peak and $0\,\text{dBm}$ average power, the SI signal is cancelled to the $-90\,\text{dBm}$ noise floor by applying both RF SIC and the digital SIC algorithm described before. Fig. 6 shows the screenshot of the NI LabVIEW front panel visualizing the transmitted and received signals at one FD transceiver, in both time and frequency domains. In particular, the ferrite circulator and the conventional RF SI canceller together provide $40\,\text{dB}$ SI suppression before the USRP RX, of which around $20\,\text{dB}$ is obtained from the RF SI canceller. The additional $50\,\text{dB}$ suppression comes from the digital SIC which eventually allows us to detect the desired signal under the powerful SI.

V. Conclusion

We discussed the challenges imposed by the design of IC-based FD systems and presented some of the results obtained within the FlexICoN project [13]. The recent results demonstrate that FD is a promising wireless technology with great potential for improving the spectrum efficiency. Hence, we believe that FD will soon become part of 5G wireless standards, leading to higher rates and more flexible spectrum use in wireless networks and systems.

VI. Acknowledgments

This research was supported in part by the NSF grant ECCS-1547406, DARPA RF-FPGA program HR0011-12-1-0006, Qualcomm Innovation Fellowship, and the People Programme (Marie Curie Actions) of the European Union's Seventh Framework Programme (FP7/2007-2013) under REA grant agreement n°[PIIF-GA-2013-629740].11.

References

[1] L. J. Young, "Telecom experts plot a path to 5G," *IEEE Spectrum*, vol. 52, no. 10, pp. 14–15, 2015.

[2] A. Sabharwal, P. Schniter, D. Guo, D. Bliss, S. Rangarajan, and R. Wichman, "In-band full-duplex wireless: Challenges and opportunities," *IEEE J. Sel. Areas Commun.*, vol. 32, no. 9, pp. 1637–1652, Sept. 2014.

[3] D. Bharadia, E. McMilin, and S. Katti, "Full duplex radios," in *Proc. ACM SIGCOMM'13*, 2013.

[4] M. Duarte, C. Dick, and A. Sabharwal, "Experiment-driven characterization of full-duplex wireless systems," *IEEE Trans. Wireless Commun.*, vol. 11, no. 12, pp. 4296–4307, Dec. 2012.

[5] M. Chung, M. S. Sim, J. Kim, D. K. Kim, and C. b. Chae, "Prototyping real-time full duplex radios," *IEEE Commun. Mag.*, vol. 53, no. 9, pp. 56–63, Sept. 2015.

[6] J. Zhou, A. Chakrabarti, P. Kinget, and H. Krishnaswamy, "Low-noise active cancellation of transmitter leakage and transmitter noise in broadband wireless receivers for FDD/co-existence," *IEEE J. Solid-State Circuits*, vol. 49, no. 12, pp. 1–17, Dec. 2014.

[7] J. Zhou, T. H. Chuang, T. Dinc, and H. Krishnaswamy, "Integrated wideband self-interference cancellation in the RF domain for FDD and full-duplex wireless," *IEEE J. Solid-State Circuits*, vol. 50, no. 12, pp. 3015–3031, Dec. 2015.

[8] J. Zhou, N. Reiskarimian, and H. Krishnaswamy, "Receiver with integrated magnetic-free N-path-filter-based non-reciprocal circulator and baseband self-interference cancellation for full-duplex wireless," in *Proc. IEEE ISSCC'16*, 2016.

[9] T. Dinc and H. Krishnaswamy, "A T/R antenna pair with polarization-based wideband reconfigurable self-interference cancellation for simultaneous transmit and receive," in *Proc. IEEE IMS'15*, 2015.

[10] T. Dinc, A. Chakrabarti, and H. Krishnaswamy, "A 60 GHz CMOS full-duplex transceiver and link with polarization-based antenna and RF cancellation," *IEEE J. Solid-State Circuits*, vol. 51, no. 5, pp. 1125–1140, May 2016.

[11] D. J. van den Broek, E. A. M. Klumperink, and B. Nauta, "An in-band full-duplex radio receiver with a passive vector modulator downmixer for self-interference cancellation," *IEEE J. Solid-State Circuits*, vol. 50, no. 12, pp. 3003–3014, Dec. 2015.

[12] D. Yang, H. Yuksel, and A. Molnar, "A wideband highly integrated and widely tunable transceiver for in-band full-duplex communication," *IEEE J. Solid-State Circuits*, vol. 50, no. 5, pp. 1189–1202, May 2015.

[13] "The Columbia FlexICoN project," http://flexicon.ee.columbia.edu/.

[14] B. Debaillie, D.-J. van den Broek, C. Lavin, B. van Liempd, E. Klumperink, C. Palacios, J. Craninckx, B. Nauta, and A. Parssinen, "Analog/RF solutions enabling compact full-duplex radios," *IEEE J. Sel. Areas Commun.*, vol. 32, no. 9, pp. 1662–1673, Sept. 2014.

[15] E. Yetisir, C.-C. Chen, and J. Volakis, "Low-profile UWB 2-port antenna with high isolation," *IEEE Antennas and Wireless Propagation Letters*, vol. 13, pp. 55–58, 2014.

[16] A. Wegener and W. Chappell, "High isolation in antenna arrays for simultaneous transmit and receive," in *IEEE International Symposium on Phased Array Systems Technology*, 2013.

[17] A. Wegener, "Broadband near-field filters for simultaneous transmit and receive in a small two-dimensional array," in *Proc. IEEE IMS'14*, 2014.

[18] B. van Liempd, B. Hershberg, K. Raczkowski, S. Ariumi, U. Karthaus, K. F. Bink, and J. Craninckx, "A +70dbm IIP3 single-ended electrical-balance duplexer in 0.18um SOI CMOS," in *Proc. IEEE ISSCC'15*, 2015.

[19] N. Reiskarimian and H. Krishnaswamy, "Magnetic-free non-reciprocity based on staggered commutation," *Nat. Commun.*, vol. 7, no. 4, Apr. 2016.

[20] A. Ghaffari, E. A. M. Klumperink, M. C. M. Soer, and B. Nauta, "Tunable high-Q N-path band-pass filters: Modeling and verification," *IEEE J. Solid-State Circuits*, vol. 46, no. 5, pp. 998–1010, May 2011.

[21] J. Marašević, J. Zhou, H. Krishnaswamy, Y. Zhong, and G. Zussman, "Resource allocation and rate gains in practical full-duplex systems," *IEEE/ACM Trans. Netw. (to appear)*, 2016.

[22] J. Zhou, J. Marašević, H. Krishnaswamy, and G. Zussman, "Co-design of full-duplex rfic and resource allocation algorithms," in *IEEE Power Amplifier Symposium*, 2015.

[23] J. Marašević and G. Zussman, "On the capacity regions of single-channel and multi-channel full-duplex links," in *Proc. ACM MobiHoc'16*, 2016.

[24] T. Chen, J. Zhou, N. Grimwood, R. Fogel, J. Marašević, H. Krishnaswamy, and G. Zussman, "Demo: Full-duplex wireless based on a small-form-factor analog self-interference canceller," in *Proc. ACM MobiHoc'16*, 2016.